Chemistry SELECT

www.chemistryselect.org

A journal of ChemPubSoc Europe

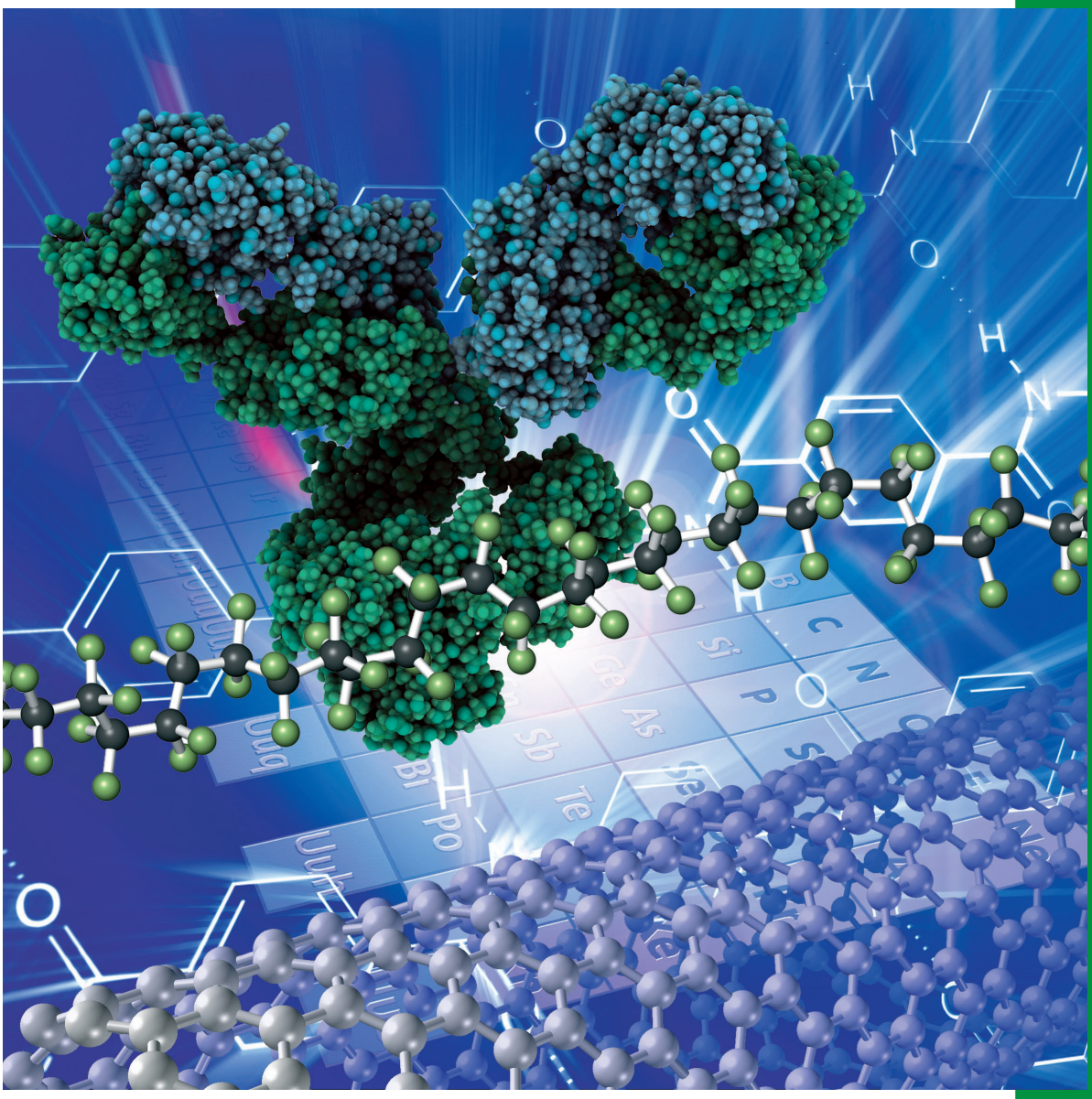

REPRINT

WILEY-VCH

ChemPubSoc Europe

DOI: 10.1002/slct.201901175

Chemistry SELECT Full Papers

Materials Science inc. Nanomaterials & Polymers

Optimization of Synthesis Parameters for the Production of Biphasic Calcium Phosphate Ceramics via Wet Precipitation and Sol-Gel Process

Rémi G. Tilkin,*[a, b] Julien G. Mahy,[a] Nicolas Régibeau,[a, b] Christian Grandfils,[b] and Stéphanie D. Lambert[a]

During the past few years, bioceramics, like hydroxyapatite and β-tricalcium phosphate have been widely developed for bone reconstruction. These materials have to meet strict criteria regarding biocompatibility, degradability, and mechanical properties. This work has been focusing on the influence of synthesis parameters on the production of calcium phosphate mixes, called biphasic calcium phosphate. In this optic, powders obtained from two synthesis processes (*i.e.* wet precipitation and sol-gel process) were produced. The influence of pH, Ca/P molar mixing ratio, and calcination temperature was studied. These new materials were characterized in terms of composition, thermal properties, and textural properties via X-ray diffraction, infrared spectroscopy, scanning electronic microscopy, thermogravimetric analysis, and nitrogen adsorption-desorption. Wet precipitation technique produces *in situ* mixes with different hydroxyapatite contents while the sol-gel process ends up with ceramics contaminated by cytotoxic CaO. Wet precipitation has been demonstrated more successful to control *in situ* mixes with specific composition.

Introduction

Bone possesses the capacity of self-regeneration allowing its repair without any scar.[1,2] However, this self-repairing ability presents some limit, explaining that for large fracture defects (*i.e.* gap beyond two and a half times the bone radius), assistance is needed in order to recover the complete structure and function of the native bone.[3] It is notably the case for up to 13% of tibia fractures related to delayed union or fracture non-union.[4] During the past few years, tissue engineering has become one of the most promising techniques to maintain, improve, or reconstruct human tissue, even complete human organs.[5–7] This approach is frequently based on the realization of temporary porous matrices, also called "scaffolds".[5–8] These materials are highly porous matrices designed to architecture the development of cells in order to guarantee an improved functionality of the implant during the regeneration process.

Several materials have been proposed for the conception of scaffolds, including calcium phosphate ceramics.[9,10] Among these materials, the bioceramic class is notably composed of hydroxyapatite (HA), $Ca_{10}(PO_4)_6(OH)_2$ (Ca/P molar ratio = 1.67), and β-tricalcium phosphate (β-TCP), β-$Ca_3(PO_4)_2$ (Ca/P molar ratio = 1.5). Both products are frequently used because of their biomimetism. Their chemical and structural similarity to human bones explain good scores observed *in vitro* and *in vivo* in terms of biocompatibility and osteoconductivity (*i.e.* cell colonization).[11,12] HA/β-TCP mixes, called biphasic calcium phosphate (BCP, theoretical Ca/P molar ratio between 1.5 and 1.67) have gained increasing importance in the past years.[9] BCP have been studied in order to combine suitable mechanical properties, from the HA component, and good kinetics of biodegradability, from the β-TCP component. These properties greatly depends on BCP composition (*i.e.* HA/β-TCP ratio).[13–16] Biocompatibility is also influenced by BCP composition.[16,17] Therefore, a simple and systematic synthesis process is required to produce BCP with various HA/β-TCP ratios in a controllable way.

Several methods have already been proposed for the synthesis of BCP, including hydrothermal technique, flame spray, wet precipitation, and sol-gel process.[9,13,18,19] Amongst them, wet precipitation (WP) is the most commonly used technique due to the simplicity of experimental operations, the low operating temperature, and its high yield.[20–22] However, wet precipitation suffers from lack of reproducibility during the synthesis process due to insufficient control of pH, temperature or Ca/P molar ratio, resulting in differences in terms of stoichiometry or morphology.[22] On the other hand, sol-gel process (SG) has gained great interest because of the homogeneous molecular mixing, the low processing temperature, the control of particle size, and the ability to improve the contact and stability at the artificial/natural bone interface.[23–25] Moreover, this technique presents practical advantages such as the simplicity of equipment used, the low installation cost, and

[a] R. G. Tilkin, Dr. J. G. Mahy, N. Régibeau, Prof. Dr. S. D. Lambert
Department of Chemical Engineering – Nanomaterials, Catalysis, Electrochemistry (NCE)
University of Liège
Allée du Six Août 11, 4000 Liège, Belgium
E-mail: rtilkin@uliege.be

[b] R. G. Tilkin, N. Régibeau, Dr. C. Grandfils
Centre Interfacultaire des Biomatériaux (CEIB)
University of Liège
Allée du Six Août 11, 4000 Liège, Belgium

Supporting information for this article is available on the WWW under https://doi.org/10.1002/slct.201901175

the flexibility to produce different solid forms (*e.g.* powder, bulk amorphous monolith, thin films).[23]

Previous studies showed a clear mismatch between exhibited characteristics and manufacturer specifications as well as a lack of reproducibility between suppliers.[26] To tackle this problem, calcium phosphate ceramics have already been produced by wet precipitation and sol-gel process.[14,27–33] However, our literature survey highlighted that limited information was available regarding the effect of synthesis methods and parameters on powder composition and porosity. Even if the comparison between WP and SG techniques has already been studied, these studies lacked a systematic analysis of the synthesis parameters.[34,35] This study focused on the influence of the synthesis parameters on the composition of calcium phosphate ceramics for the production of pure HA, pure β-TCP, and BCP. In this optic, powders were obtained from two synthesis processes (*i.e.*wet precipitation and sol-gel process) and the influence of different parameters (*i.e.* pH, Ca/P molar mixing ratio, calcination temperature) on powder composition was studied in a systematic manner. These new materials were then characterized via X-ray diffraction (XRD), infrared spectroscopy (FTIR), scanning electronic microscopy (SEM), thermogravimetric analysis (TGA), and nitrogen adsorption-desorption.

Results and Discussion

The aim of this study was the synthesis of several calcium phosphate ceramics (*i.e.* pure HA, pure β-TCP, and BCP) for bone reconstruction applications. In this optic, two synthesis methods were used: wet precipitation (marked as WP) and sol-gel process (marked as SG). Several synthesis parameters were studied: pH (*i.e.* 8 or 10 for WP samples and 10 or unfixed for SG samples), Ca/P molar mixing ratio (*i.e.* from 1.5 to 1.7), calcination temperature (*i.e.* from 700 to 900 for WP samples and from 600 to 1000 for SG samples). The different synthesis conditions are presented in Table S1 in the Supporting Information. These new materials were characterized via XRD (*i.e.* composition and crystallinity), FTIR (*i.e.* composition), TGA (*i.e.* thermal analysis), and SEM (*i.e.* morphology)

From a macroscopic point of view, the two synthesis processes produce two different types of powders. On one hand, the wet precipitation process produces white powders. When a stoichiometric Ca/P molar mixing ratio is used, HA precipitates from the supersaturated solution containing Ca^{2+} and PO_4^{3-} ions (see Equation (1)).[21]

$$10\ Ca(NO_3)_2 + 6\ (NH_4)_2HPO_4 + 8\ NH_4OH \rightarrow Ca_{10}(PO_4)_6(OH)_2 + 20\ NH_4NO_3 + 6\ H_2O \quad (1)$$

When a lower Ca/P molar mixing ratio (*i.e.* between 1.5 and 1.67), calcium-deficient hydroxyapatite precipitates according to the reaction presented in Equation (2).

$$9\ Ca(NO_3)_2 + 6\ (NH_4)_2HPO_4 + 6\ NH_4OH \rightarrow Ca_9(HPO_4)(PO_4)_5(OH) + 18\ NH_4NO_3 + 5\ H_2O \quad (2)$$

$(NH_4)_2HPO_4$ is considered in the reactions because HPO_4^{2-} is the major species present at pH 8 and pH 10.[36] $Ca(NO_3)_2$ and H_3PO_4 were chosen as reagents because the byproduct produced (*i.e.* NH_4NO_3) is easily removed or decomposed. Furthermore, it has been shown that NH_4^+ and NO_3^- ions are not incorporated into the HA lattice.[37] As presented later (see Equation (8)), β-TCP results from the decomposition of calcium-deficient hydroxyapatite at high temperature.

On the other hand, the sol-gel process produces gray powders, indicating the presence of organic compounds. This color becomes lighter when increasing the calcination temperature from 600 °C to 900 °C, showing a decrease in the organic content. At 1000 °C, white powder is obtained. HA is formed during the ageing step via the reaction presented in Equation (3).[38]

$$10\ Ca(CH_3COO)_2 + 20\ H_2O + 6\ P(OEt)_3(O) \rightarrow 18\ C_2H_5OH + Ca_{10}(PO_4)_6(OH) + 20\ CH_3COOH \quad (3)$$

Composition and crystallinity analysis via XRD

XRD patterns of calcined powders and compositions (assessed via Rietveld refinement) are shown in Figures 1 and 2, and Tables 1 and 2. Regarding wet precipitation process (Figure 1),

Table 1. Composition of samples synthesized via the wet precipitation method.

Sample	HA [wt%]	β-TCP [wt%]	α-TCP [wt%]	Exp. Ca/P ratio
WP_1 700	100			1.67
WP_1 800	100			1.67
WP_1 900	100			1.67
WP_2 700	89	11		1.65
WP_2 800		100		1.50
WP_2 900		100		1.50
WP_3	82	8	10	1.64
WP_4	52	48		1.58
WP_5		100		1.50
WP_6	11	89		1.52

Table 2. Composition of samples synthesized via the sol-gel method.

Sample	HA [wt%]	$CaCO_3$ [wt%]	CaO [wt%]	$Ca(OH)_2$ [wt%]	Exp. Ca/P ratio
SG_1 600	67	33			2.49
SG_1 900	80		20		2.41
SG_1 1000	80		7	13	2.29
SG_2	18		74	8	12.29
SG_3	84		16		2.24

in situ HA/TCP mixes are detected (ICDD # 00–064-0738 for HA, # 00–055-0898 for β-TCP, and # 04–010-4348 for α-TCP). The composition of the BCP depends on the mixing molar ratio Ca/P, the pH, and the calcination temperature. At pH 10, Ca/P

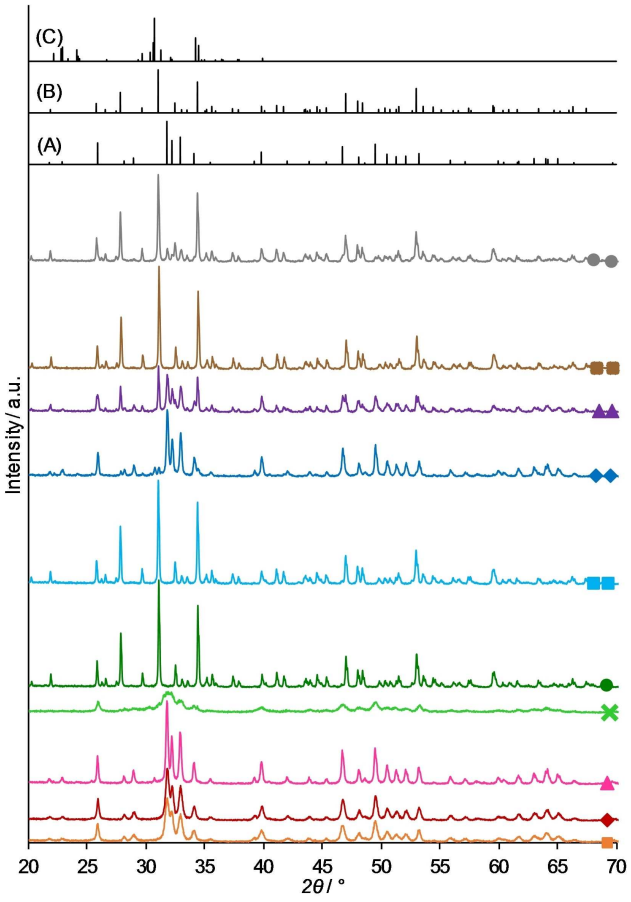

Figure 1. XRD patterns of samples synthesized via wet precipitation method: ■ WP_1 700, ♦ WP_1 800, ▲ WP_1 900, ×× WP_2 700, ● WP_2 800, ■■ WP_2 900, ♦♦ WP_3 900, ▲▲ WP_4 900, ×× WP_5 900, ●● WP_6 900. Reference XRD patterns: (A) HA (B) β-TCP (C) α-TCP.

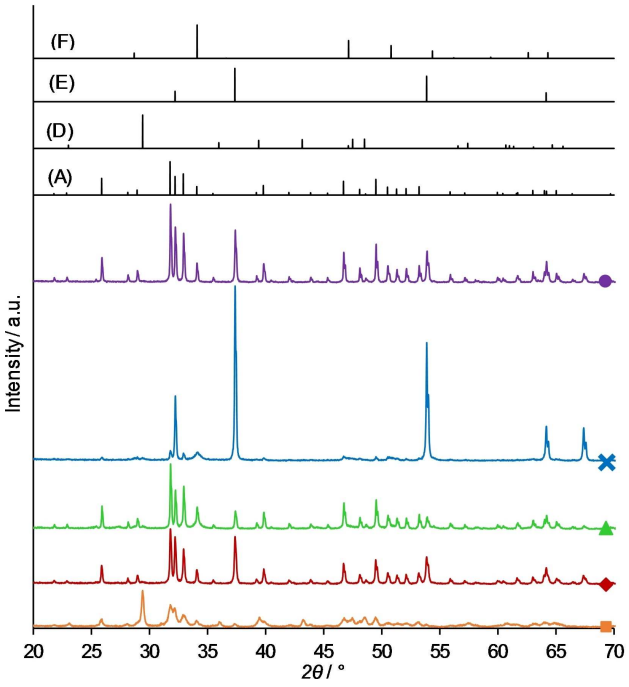

Figure 2. XRD patterns of samples synthesized via sol gel process: ■ SG_1 600, ♦ SG_1 900, ▲ SG_1 1000, × SG_2 1000, ● SG_3 1000. Reference XRD patterns: (A) HA (D) $CaCO_3$ (E) CaO (F) $Ca(OH)_2$.

molar mixing ratio equal to 1.7 (*i.e.* WP_1) produces pure HA. On the other hand, pure β-TCP is obtained using Ca/P molar mixing ratio equals to 1.5 (*i.e.* WP_5). Gradually decreasing Ca/P ratio between 1.7 and 1.5 (*i.e.* WP_3 and WP_4) leads to the formation of BCP containing a decreasing percentage of HA. Interestingly, the use of the theoretical Ca/P molar mixing ratio to obtain pure HA (*i.e.* Ca/P = 1.67, WP_3) also produces α-TCP and β-TCP. The presence of α-TCP is not a problem since this compound is biocompatible and biodegradable.[39] It is thought that in order to produce pure HA, calcium solution should be used in slight excess in order to compensate for experimental losses during addition and mixing. Altering the pH during the mixing step also affects BCP composition. Decreasing the pH from 10 to 8 while maintaining a constant Ca/P molar mixing ratio of 1.7 (*i.e.* WP_6) greatly increases the percentage of β-TCP in the sample. In the case of a Ca/P molar mixing ratio of 1.5 (*i.e.*, WP_2), the pH decrease does not affect the BCP composition compared to WP_5. The calcination temperature also has an impact on the mix composition. It can be observed that the HA peaks of WP_1 become narrower as the calcination temperature increases from 700 to 900 °C, indicating an increase of the elementary crystallite size. This trend is confirmed by the crystallite size of HA calculated via Scherrer equation: 27 nm at 700 °C, 40 nm at 800 °C, and 59 nm at 900 °C. Regarding WP_2, HA can be detected up to 700 °C while only β-TCP can be observed at 800 °C and 900 °C. These results indicate that the transformation of HA to β-TCP occurs between 700 and 800 °C. An advantage of this *in situ* synthesis is a mixing at the crystallite scale, which is impossible to realize with simple mixing. Indeed, reduction of the mean particle size is not always possible. It has notably been shown that α-TCP and β-TCP particles, generally produced by high-temperature solid-state reactions and milling, do not become smaller during prolonged milling but amorphous.[40,41] *In situ* synthesis also prevents a possible phase separation process.

In the case of the sol-gel process (Figure 2), HA/$CaCO_3$ or HA/CaO mixes are obtained (ICDD # 00–005-0586 for $CaCO_3$, # 00–037-1497 for CaO, and # 01–078-0315 for $Ca(OH)_2$). As for wet precipitation, the mixing molar ratio Ca/P, the pH, and the calcination temperature influence the composition of the BCP. A high content of HA (*i.e.* 80–84% HA for SG_1 and SG_3) can be produced by using a Ca/P molar mixing ratio of 1.67. On the other hand, a Ca/P molar mixing ratio of 1.5 leads to the formation of powder containing a small proportion of HA (*i.e.* 18% HA for SG_2). It can be seen from SG_3 results that increasing the pH at the beginning of the mixing step only has a small effect of the proportion of HA in the resulting powder. As already mentioned, the calcination temperature influences the nature of the phases. Indeed, $CaCO_3$ is detected in SG_1 sintered at 600 °C while CaO is found in ceramic sintered at 900 °C and over. $CaCO_3$ probably results from the decomposi-

tion of the excess of $Ca(CH_3COO)_2$ and the combustion of organic compounds such as unreacted $PO(OC_2H_5)_3$, products of $PO(OC_2H_5)_3$ hydrolysis or remaining solvent.[33,42] $CaCO_3$ is then decomposed into CaO between 600 and 900 °C. CaO has been proven cytotoxic.[43,44] It has been shown that CaO inhibits the *in vivo* formation of bone in close proximity to the implant. This phenomenon results from the hydration of CaO in the physiological environment via the reaction presented in Equation 4.

$$CaO + H_2O \rightarrow Ca(OH)_2 \quad (4)$$

The formation of $Ca(OH)_2$ leads to an elevation of the local pH around the implant, which is detrimental to the surrounding cells. For this reason, CaO and $Ca(OH)_2$ should be removed before use for biomedical applications. This reaction also explained the presence of $Ca(OH)_2$ in SG_2, resulting from the reaction of CaO with atmospheric water. It can also be observed that the HA peaks of SG_1 become narrower as the calcination temperature increases from 600 to 1000 °C, indicating an increase of the elementary crystallite size. This trend is confirmed by the crystallite size of HA calculated via Scherrer equation: 38 nm for 600 °C, 80 nm at 900 °C and 89 nm at 1000 °C, which is larger than what can be obtained via wet precipitation.

Composition analysis via FTIR

The corresponding FT-IR absorption spectra of the sintered calcium phosphate powders are displayed in Figures 3 and 4. FTIR spectra of WP samples exhibit characteristic peaks of HA and β-TCP. The peaks corresponding to the bending of PO_4^{3-} groups are observed at 559–561 and 598–600 cm^{-1} for HA and at 542–544, 571, 579, 588–590, and 600–604 cm^{-1} for β-TCP.[45–49] The stretching of PO_4^{3-} groups is detected at 962, 1022–1024, and 1086–1088 cm^{-1} for HA and at 970, 1013–1016, 1078, 1099, and 1115 cm^{-1} for β-TCP.[39,49,50] Characteristic peaks of structural OH^- are present at 629–631 and 3578 cm^{-1}.[47,50] Confirming the XRD results regarding the effect of Ca/P molar mixing ratio and pH on the BCP composition, HA is detected for WP_1, WP_2 (under 700 °C), WP_3, and WP_4, while β-TCP is present in WP_2 (above 700 °C), WP_5, and WP_6. As for XRD patterns, the calcination temperature has an impact on FTIR spectra. It can be seen that the peak intensity of WP_1 spectra increases with calcination temperature. For WP_2, the peak assigned to HPO_4^- (*i.e.* 880 cm^{-1}) was detected for BCP sintered at 700 °C, indicating the presence of calcium-deficient HA, $Ca_9(HPO_4)(PO_4)_5(OH)$.[46] This peak disappears for powder sintered at higher temperature, leaving only β-TCP. This also suggests that the transformation of HA to β-TCP occurs between 700 and 800 °C.

Regarding SG samples, FTIR spectra also confirm the results obtained via XRD patterns. Characteristic peaks corresponding to HA/$CaCO_3$ or HA/CaO mixes are detected. However, β-TCP is not found in the SG samples. As for WP samples, the peaks corresponding to the bending of PO_4^{3-} groups are observed at 565–567, 574, and 598–602 cm^{-1}.[46,49] The stretching of PO_4^{3-} groups is detected at 962–964, 1026–1032, and 1087–1092 cm^{-1}.[39,46,47,49] Characteristic peaks of structural OH^- are present at 629–633 and 3572–3578 cm^{-1}.[47,50] CaO and $Ca(OH)_2$ are also detected via a very large band starting at 660 cm^{-1} and a smaller peak at 712 cm^{-1}, which are characteristic of the Ca–O bond.[51] The peak observed at 3642–3644 cm^{-1} corresponds to the OH bonds from $Ca(OH)_2$. Peaks corresponding to

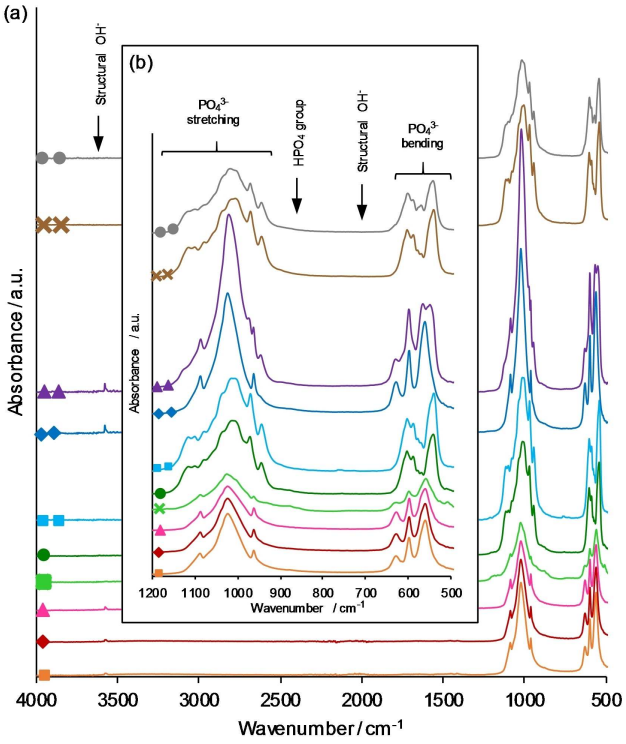

Figure 3. FTIR spectra of samples synthesized via wet precipitation method: ■ WP_1 700, ♦ WP_1 800, ▲ WP_1 900, × WP_2 700, ● WP_2 800, ■■ WP_2 900, ♦♦ WP_3 900, ▲▲ WP_4 900, ×× WP_5 900, ●● WP_6 900. (a) Full spectra (b) Focus on the fingerprint region.

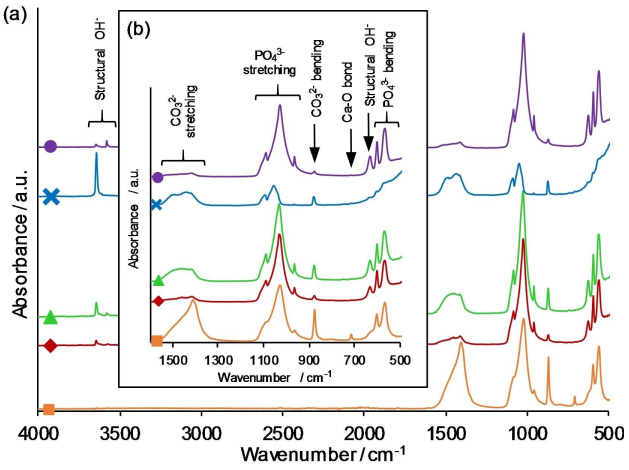

Figure 4. FTIR spectra of samples synthesized via sol gel process: ■ SG_1 600, ♦ SG_1 900, ▲ SG_1 1000, × SG_2 1000, ● SG_3 1000. (a) Full spectra (b) Focus on the fingerprint region.

the CO_3^{2-} bending and stretching are also observed respectively at 874–876 cm^{-1}, and at 1408–1418 cm^{-1} and 1456 cm^{-1}.[47] Moreover, a large band is present between 1300 and 1600 cm^{-1}. This band is attributed to the CO_3^{2-} stretching. This band varies depending on the calcination temperature (*i.e.* SG_1 600, SG_1 900, and SG_1 1000). At 600 °C, the high intensity of this band indicates the presence of $CaCO_3$ and organic compounds. These organic compounds are responsible for the gray color of the powder. At 900 °C, the intensity of this band greatly decreases, showing a decrease of the organic content. The gray color of the powder also becomes less intense. The intensity increase of the peak at 874–876 cm^{-1} and the band at 1300–1600 cm^{-1} observed at 1000 °C are probably due to the presence of B-type carbonate hydroxyapatite (B-cHA), $Ca_{10}(PO_4)_{6-x}(CO_3)_x(OH)_2$, in which some of the PO_4^{3-} ions are substituted by CO_3^{2-} ions.[33,52] Peaks with different intensities corresponding to carbonate hydroxyapatite are also present in SG_2 and SG_3. The variation of peak intensity between samples indicates that the quantity of B-cHA in each sample is different. The identification of this phase via XRD is impaired because of the superposition of the peaks corresponding the (112) peaks of B-cHA and HA.[33] Moreover, incomplete crystallization of B-cHA reduces the possibility to detect this phase.

Thermal analysis via TGA

Figure 5 illustrates the results of the thermal analysis of WP_1, WP_2, and SG_1. Regarding WP_1 and WP_2, the weight loss

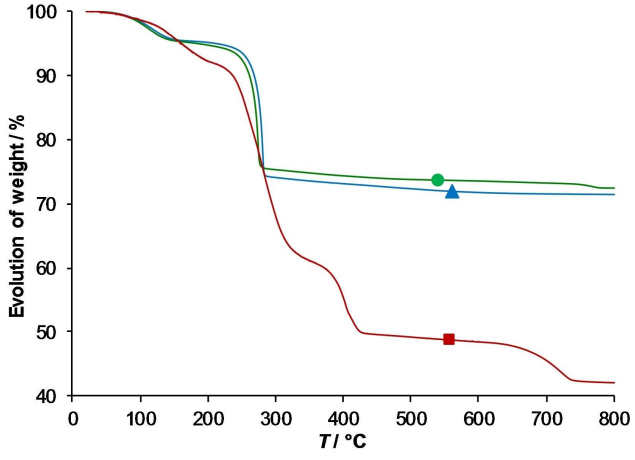

Figure 5. Thermal analysis of ■ SG_1, ▲ WP_1, ● WP_2.

between 20 and 150 °C (*i.e.* 4.5 and 4.8% respectively) can be assigned to dehydration. Between 150 and 285 °C, a sharp weight loss (*i.e.* 21.1 and 19.9% for WP_1 and WP_2 respectively) can be observed due to ammonium nitrate decomposition via the endothermic reaction presented in Equation (5)

$$NH_4NO_3 \rightleftharpoons HNO_3 + NH_3 \text{ (around 170 °C)} \quad (5)$$

and then via the exothermic reactions presented in Equation (6) and (7).[53–55]

$$NH_4NO_3 \rightarrow N_2O + 2\,H_2O \text{ (between 170 and 230 °C)} \quad (6)$$

$$NH_4NO_3 \rightarrow 3/4\,N_2 + 1/2\,NO_2 + 2\,H_2O \text{ (above 230 °C)} \quad (7)$$

The theoretical proportion of NH_4NO_3 in the dry sample is about 40 wt%. It can thus be seen that a large part of this compound is evacuated in the supernatant during the centrifugation. Moreover, NH_4NO_3 is decomposed at low temperature. Both reasons justified why a washing step can be avoided. The transformation of calcium-deficient HA to β-TCP is detected on WP_2 curve via a slight weight loss (*i.e.* 0.6%) between 740 and 785 °C. Based on the previous XRD and FTIR results, we can deduce that this transformation occurs through the decomposition of calcium-deficient hydroxyapatite via the reaction presented in Equation (8).[56–58]

$$Ca_9(HPO_4)(PO_4)_5(OH) \rightarrow 3\,\beta\text{-}Ca_3(PO_4)_2 + H_2O \quad (8)$$

The total weight loss for WP_1 and WP_2 at 800 °C is 28.4 and 27.6 respectively.

Regarding SG_1, a greater weight loss is observed (*i.e.* 57.9%). The weight loss between 20 and 350 °C (*i.e.* 38.9%) is attributed to loss of volatile substance, such as hydrates, remaining of solvent, and products of triethylphosphate hydrolysis.[42] Between 350 and 450 °C, the weight loss (*i.e.* 11.4%) is due to the evolution of the decomposition of calcium acetate into calcium carbonate via the reaction presented in Equation (9).[33,59]

$$Ca(CH_3COO)_2 + 4\,O_2 \rightarrow CaCO_3 + 3\,CO_2 + 3\,H_2O \quad (9)$$

The decomposition of $CaCO_3$ into CaO is detected between 620 and 750 °C (*i.e.* weight loss of 6.1%).[59,60] The transformation follows the reaction presented in Equation (10).

$$CaCO_3 \rightarrow CaO + CO_2 \quad (10)$$

Textural properties analysis via SEM and nitrogen adsorption-desorption

Figures 6 and 7 display the morphology of calcium phosphate powders. Prepared calcium phosphate ceramics present different morphologies depending on the synthesis method, the pH, and the Ca/P molar mixing ratio used. Regarding WP samples, it can be observed that the presence of TCP (*i.e.* in WP_2, WP_4, and WP_6) leads to the formation of cylindrical or spherical

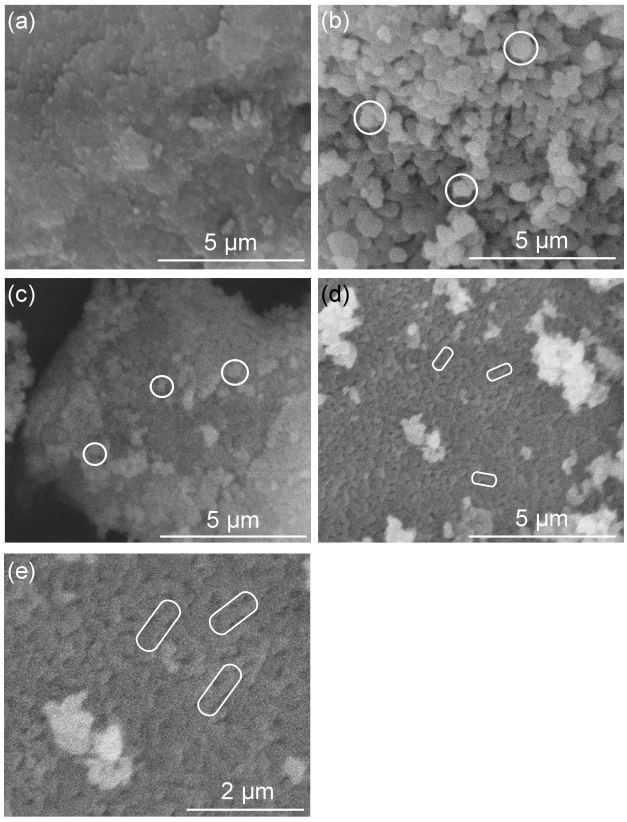

Figure 6. Morphology (SEM analysis) of samples synthesized via wet precipitation: (a) WP_1 900, (b) WP_2 900, (c) WP_4 900, (d-e) WP_6 900. Representative particle shapes are encircled.

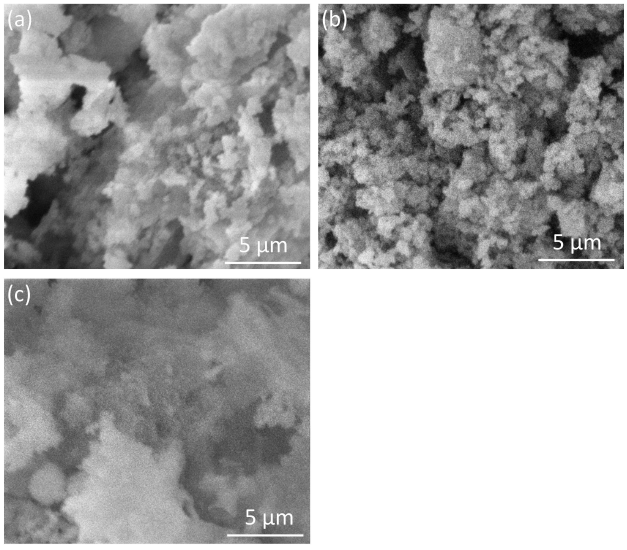

Figure 7. Morphology (SEM analysis) of samples synthesized via sol-gel process: (a) SG_1 1000, (b) SG_2 1000, (c) SG_3 1000.

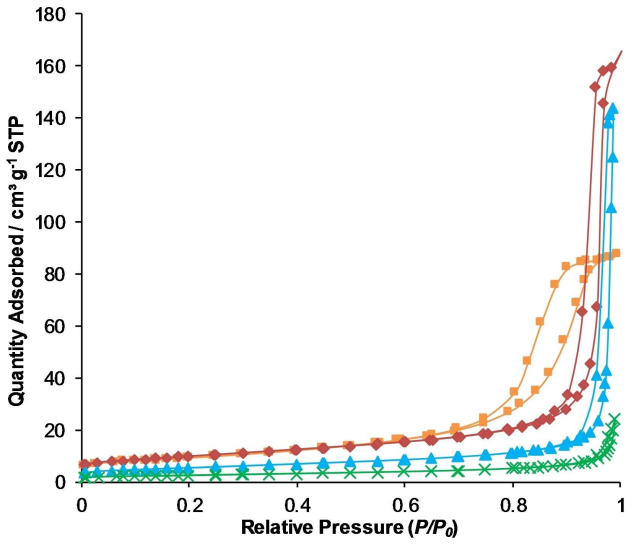

Figure 8. Nitrogen adsorption-desorption isotherms of WP_1: ■ WP_1 dry, ♦ WP_1 700, ▲ WP_1 800, × WP_1 900

grains with a size depending on the synthesis conditions. Pure β-TCP (*i.e.* WP_2) forms large spherical particles in the range of 450–650 nm. The presence of HA reduces the grain size. In the case of WP_4 (*i.e.* Ca/P molar ratio = 1.6), grains form smaller aggregates in the range of 350–450 nm. In the case of WP_6 (*i.e.* pH 10), rod-like particles with a diameter in the range of 170–220 nm and a length between 400 and 450 nm can be observed. The pH decrease is also probably responsible of this change in shape. On the other hand, in the presence of pure HA (*i.e.* WP_1), large plates are formed. On these plates, small aggregates in the range of 130–200 nm can be seen. These results are in agreement with results of the literature.[61]

As can be seen in Figure 7, the sol-gel synthesis gives rise to larger particles. As for WP samples, the synthesis parameters influence the ceramic morphology. In the case of sample containing HA in large amount (*i.e.* SG_1 and SG_3), large plates in the range of 1–1.4 µm are present which is similar to what can be observed for pure HA. On the other hand, the presence of large amount of CaO (*i.e.* SG_2) impairs the formation of these large plates. In this case, grains agglomerates to form particles between 750 and 1000 nm.

The nitrogen adsorption-desorption isotherms are depicted in Figure 8 for WP_1 and Figure 9 for WP_2. Isotherms of samples composed of BCP (*i.e.* WP_3, WP_4, WP_5, and WP_6) present a shape between these two extremes. Surface area of WP samples are given in Table 3. The porosity analysis was

Table 3. Surface Area (S_{BET}) of samples synthesized via the wet precipitation method (in $m^2\ g^{-1}$).

Sample	Dry	700 °C	800 °C	900 °C
WP_1	30	35	20	10
WP_2	30	20	5	< 5
WP_3	/	/	/	10
WP_4	/	/	/	10
WP_5	/	/	/	< 5
WP_6	/	/	/	< 5

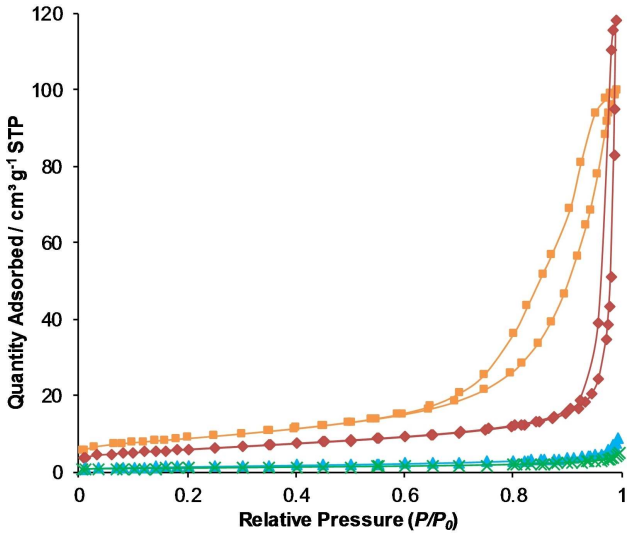

Figure 9. Nitrogen adsorption-desorption isotherms of WP_2: ■ WP_2 dry, ♦ WP_2 700, ▲ WP_2 800, × WP_2 900

focused on the samples composed of HA, TCP, or BCP, which are the main interest of this present study. Indeed, SG samples present a large proportion of cytotoxic CaO, which are harmful for the cells.

The evolution of porosity with the calcination temperature can be seen on WP_1 and WP_2. Regarding WP_1, a mixture of type II and IV isotherms according to the BDDT classification can be observed.[62] They are characterized by a quick increase of the adsorbed volume at high pressure like in type II isotherm (corresponding to macroporous solid) and by the presence of a hysteresis (type IV, mesoporous solid). The increase of the surface area after calcination at 700 °C can be explained by the degradation of NH_4NO_3 present in the HA matrix (as could be seen in Figure 5), which creates more porosity. Sintering then occurs, which leads to a reduction of the surface area and an increase in the mesoporous pore size (shift of the hysteresis towards higher pressure). At 900 °C, the surface area becomes low and the solid becomes almost exclusively macroporous. The influence of the calcination temperature on the microporosity of calcium phosphate ceramics are consistent with results present in the literature.[16,26] Regarding WP_2 samples, comparable observation can be realized. WP_2 dried and WP_2 700 present a mixture of type II and IV isotherms according to the BDDT classification.[62] The decrease in surface area between these samples can be explained by the presence of β-TCP that is hardly porous.[63] After 800 °C, the conversion of calcium-deficient HA to β-TCP reduces the porosity. WP_3 and WP_4 present a remaining porosity comparable to the one of WP_1 after calcination at 900 °C because of the presence of a large proportion of HA. On the other hand, WP_5 and WP_6 present a very low remaining porosity like WP_1 because of the large proportion of β-TCP in their composition.

Conclusions

In conclusion, pure HA, pure β-TCP, and *in situ* HA/β-TCP mixes were prepared according to two synthesis processes in order to tune precisely the mechanical properties and the biodegradation rate of ceramic scaffolds. Regarding wet precipitation, results indicate that *in situ* mixes of HA/TCP with different HA content can be obtained. The composition depends on the Ca/P molar mixing ratio, the pH, and the calcination temperature. pH equal to 10 and Ca/P molar mixing ratio close to 1.7 tends to produce pure HA while lower pH value (*i.e.* 8) combined with Ca/P molar mixing ratio close to 1.5 give rise to pure β-TCP. By tuning pH values and Ca/P molar ratio between both extremes, *in situ* HA/β-TCP mixes with different HA content can be obtained. From a practical point of view, this technique is very promising in producing *in situ* HA/TCP mixes with specific composition for bone reconstruction applications.

Regarding the sol-gel process, HA/$CaCO_3$ or HA/CaO are produced, depending on the calcination temperature. β-TCP could not be produced using this method. As for wet precipitation samples, the Ca/P molar mixing ratio, the pH, and the calcination temperature greatly influence ceramic composition. A large amount of HA is obtained with a Ca/P molar mixing ratio of 1.67 while CaO is mainly formed when the Ca/P molar mixing ratio is reduced to 1.5. Because of their cytotoxicity, CaO and $Ca(OH)_2$ should be eliminated before being used for biomedical applications. Moreover, results indicate the presence of B-type carbonated hydroxyapatite.

Supplementary Information Summary

Supporting information contains the experimental section.

Acknowledgements

Rémi G. Tilkin and Nicolas Régibeau benefit from funding of the Fund for Scientific Research (FNRS) under a Fund for Research Training in Industry and Agriculture (FRIA) grant. Stéphanie D. Lambert also thanks FRS-FNRS for her Senior Research Associate position. The authors thank the Engineering School of the University of Liège for the grant HELP B FRIA.

Conflict of Interest

The authors declare no conflict of interest.

Keywords: Calcium phosphate ceramics · Ceramics · Gels · Precipitation · Sol-gel processes

[1] R. Dimitriou, E. Jones, D. McGonagle, P. V. Giannoudis, *BMC Med.* **2011**, *9*.
[2] M. Wang, N. Yang, *Med. Eng. Phys.* **2017**, *48*, 90–102.
[3] J. E. Schroeder, R. Mosheiff, *Injury* **2011**, *42*, 609–613.
[4] L. Audigé, D. Griffin, M. Bhandari, J. Kellam, T. P. Rüedi, *Clin. Orthop. Relat. Res.* **2005**, 221–232.
[5] C. Norotte, F. Marga, L. Niklason, G. Forgacs, *Biomaterials* **2009**, *30*, 5910–5917.

[6] M. S. Lopes, A. L. Jardini, R. M. Filho, *Chem. Eng. Trans.* **2014**, *38*, 331–336.
[7] I. Schleicher, A. Parker, D. Leavesley, R. Crawford, Z. Upton, Y. Xiao, *Tissue Eng* **2005**, *11*, 1688–1698.
[8] T. Billiet, M. Vandenhaute, J. Schelfhout, S. Van Vlierberghe, P. Dubruel, *Biomaterials* **2012**, *33*, 6020–6041.
[9] M. H. Hong, S. M. Kim, Y. K. Lee, *J. Ceram. Sci. Technol.* **2017**, *8*, 541–546.
[10] V. Kalaiselvi, R. Mathammal, P. Anitha, *J. Biotechnol. Biomater.* **2017**, *7*.
[11] M. Boutinguiza, J. Pou, R. Comesaña, F. Lusquiños, A. De Carlos, B. León, *Mater. Sci. Eng. C* **2012**, *32*, 478–486.
[12] K. Yang, J. Zhang, X. Ma, Y. Ma, C. Kan, H. Ma, Y. Li, Y. Yuan, C. Liu, *Mater. Sci. Eng. C* **2015**, *56*, 37–47.
[13] S. H. Kwon, Y. K. Jun, S. H. Hong, H. E. Kim, *J. Eur. Ceram. Soc.* **2003**, *23*, 1039–1045.
[14] J. Chen, Y. Wang, X. Chen, L. Ren, C. Lai, W. He, Q. Zhang, *Mater. Lett.* **2011**, *65*, 1923–1926.
[15] M. Descamps, L. Boilet, G. Moreau, A. Tricoteaux, J. Lu, A. Leriche, V. Lardot, F. Cambier, *J. Eur. Ceram. Soc.* **2013**, *33*, 1263–1270.
[16] G. Daculsi, R. Z. Legeros, G. Grimandi, A. Soueidan, E. Goyenvalle, J. Legeros, *Key Eng. Mater.* **2008**, 1139–1142.
[17] J. M. Bouler, P. Pilet, O. Gauthier, E. Verron, *Acta Biomater.* **2017**, *53*, 1–12.
[18] D. Mohn, N. Doebelin, S. Tadier, R. E. Bernabei, N. A. Luechinger, W. J. Stark, M. Bohner, *J. Mater. Chem.* **2011**, *21*, 13963–13972.
[19] Sunarso, A. F. Mohd Noor, S. R. Kasim, R. Otman, I. D. Ana, K. Ishikawa, *J. Biomater. Nanobiotechnol.* **2013**, *4*, 273–278.
[20] W. Feng, L. Mu-Sen, L. Yu-Peng, Q. Yong-Xin, *Mater. Lett.* **2005**, *59*, 916–919.
[21] L. B. Kong, J. Ma, F. Boey, *J. Mater. Sci.* **2002**, *37*, 1131–1134.
[22] K. Salma, L. Berzina-Cimdina, N. Borodajenko, *Process. Appl. Ceram.* **2010**, *4*, 45–51.
[23] K. Agrawal, G. Singh, D. Puri, S. Prakash, *J. Miner. Mater. Charact. Eng.* **2011**, *10*, 727–734.
[24] G. Bezzi, G. Celotti, E. Landi, T. M. G. La Torretta, I. Sopyan, A. Tampieri, *Mater. Chem. Phys.* **2003**, *78*, 816–824.
[25] F. Bakan, O. Laçin, H. Sarac, *Powder Technol.* **2013**, *233*, 295–302.
[26] M. B. Conz, J. M. Granjeiro, G. de A. Soares, *J. Appl. Oral Sci.* **2005**, *13*, 136–140.
[27] J. Katić, M. Metikoš-Huković, R. Babić, M. Marciuš, *Int. J. Electrochem. Sci.* **2013**, *8*, 1394–1408.
[28] I. Sopyan, S. Ramesh, N. A. Nawawi, A. Tampieri, S. Sprio, *Ceram. Int.* **2011**, *37*, 3703–3715.
[29] S.-H. Kwon, Y.-K. Jun, S.-H. Hong, H.-E. Kim, *J. Eur. Ceram. Soc.* **2003**, *23*, 1039–1045.
[30] R. Ramírez-Agudelo, K. Scheuermann, A. Gala-garcía, A. P. F. Monteiro, A. D. Pinzón-García, M. E. Cortés, R. D. Sinisterra, *Mater. Sci. Eng. C* **2018**, *83*, 25–34.
[31] J. Marchi, P. Greil, J. C. Bressiani, A. Bressiani, F. Müller, *Int. J. Appl. Ceram. Technol.* **2009**, *6*, 60–71.
[32] F. Gervaso, F. Scalera, S. Kunjalukkal Padmanabhan, A. Sannino, A. Licciulli, *Int. J. Appl. Ceram. Technol.* **2012**, *9*, 507–516.
[33] A. Jillavenkatesa, R. A. Condrate, *J. Mater. Sci.* **1998**, *33*, 4111–4119.
[34] C. Guzmán Vázquez, C. Piña Barba, N. Munguía, *Rev. Mex. Fis.* **2005**, *51*, 284–293.
[35] R. Ghosh, R. Sarkar, *Mater. Sci. Eng. C* **2016**, *67*, 345–352.
[36] S. Aksu, *J. Electrochem. Soc.* **2009**, *156*, C387–C394.
[37] T. V. Safronova, *Glas. Ceram.* **2009**, *66*, 136–139.
[38] U. Anjaneyulu, D. K. Pattanayak, U. Vijayalakshmi, *Mater. Manuf. Process.* **2015**, *31*, 206–216.
[39] R. G. Carrodeguas, S. De Aza, *Acta Biomater.* **2011**, *7*, 3536–3546.
[40] U. Gbureck, J. E. Barralet, L. Radu, H. G. Klinger, R. Thull, *J. Am. Ceram. Soc.* **2004**, *87*, 1126–1132.
[41] U. Gbureck, T. Hölzel, U. Klammert, K. Würzler, F. A. Müller, J. E. Barralet, *Adv. Funct. Mater.* **2007**, *17*, 3940–3945.
[42] M. F. Hsieh, L. H. Perng, T. S. Chin, H. G. Perng, *Biomaterials* **2001**, *22*, 2601–2607.
[43] H. Eshtiagh-Hosseini, M. R. Housaindokht, M. Chahkandi, *Mater. Chem. Phys.* **2007**, *106*, 310–316.
[44] K. A. Hing, I. R. Gibson, P. A. Revell, S. M. Best, W. Bonfield, *Key Eng. Mater.* **2001**, *192–195*, 373–376.
[45] D. dos S. Tavares, L. de O. Castro, G. D. de A. Soares, G. G. Alves, J. M. Granjeiro, *J. Appl. Oral Sci.* **2013**, *21*, 37–42.
[46] D. K. Pattanayak, R. Dash, R. C. Prasad, B. T. Rao, T. R. Rama Mohan, *Mater. Sci. Eng. C* **2007**, *27*, 684–690.
[47] R. N. Panda, M. F. Hsieh, R. J. Chung, T. S. Chin, *J. Phys. Chem. Solids* **2003**, *64*, 193–199.
[48] A. Jillavenkatesa, R. A. Condrate, *Spectrosc. Lett.* **1998**, *31*, 1619–1634.
[49] L. Nie, J. Suo, P. Zou, S. Feng, *J. Nanomater.* **2012**, *2012*.
[50] A. Costescu, I. Pasuk, F. Ungureanu, A. Dinischiotu, M. Costache, F. Huneau, S. Galaup, P. le Coustumer, D. Predoi, *Dig. J. Nanomater. Biostructures* **2010**, *5*, 989–1000.
[51] M. Galván-Ruiz, J. Hernández, L. Baños, J. Noriega-Montes, M. E. Rodríguez-García, *J. Mater. Civ. Eng.* **2009**, *21*, 694–698.
[52] E. Tkalčec, J. Popović, S. Orlić, S. Milardović, H. Ivanković, *Mater. Sci. Eng. C* **2014**, *42*, 578–586.
[53] Z. Han, S. Sachdeva, M. I. Papadaki, M. S. Mannan, *J. Loss Prev. Process Ind.* **2015**, *35*, 307–315.
[54] S. Chaturvedi, P. N. Dave, *J. Energ. Mater.* **2013**, *31*, 1–26.
[55] M. Pandeley, S. Jha, R. R. Jha, *Asian J. Chem.* **2011**, *23*, 340–344.
[56] D. R. R. Lazar, S. M. Cunha, V. Ussui, E. Fancio, N. B. de Lima, A. H. A Bressiani, *Mater. Sci. Forum* **2006**, *530–531*, 612–617.
[57] A. Massit, A. El Yacoubi, B. Chafik, E. Idrissi, K. Yamni, *IOSR J. Appl. Chem.* **2014**, *7*, 57–61.
[58] E. I. Dororhkina, S. V. Dorozhkin, *Chem. Mater.* **2002**, *14*, 4267–4272.
[59] A. W. Musumeci, R. L. Frost, E. R. Waclawik, *Spectrochim. Acta - Part A Mol. Biomol. Spectrosc.* **2007**, *67*, 649–661.
[60] C. Rodriguez-Navarro, E. Ruiz-Agudo, A. Luque, A. B. Rodriguez-Navarro, M. Ortega-Huertas, *Am. Mineral.* **2009**, *94*, 578–593.
[61] G. Daculsi, R. Z. Legeros, *in Bioceram. Their Clin. Appl.* (Ed.: T. Kokubo), Woodhead Publishing Limited, Cambridge, England, **2008**, pp. 395–423.
[62] A. Lecloux, *Mémoires Société des Sci. Liege* **1971**, *4*, 169–209.
[63] S. Vahabzadeh, J. Edgington, S. Bose, *Mater. Sci. Eng. C–Materials Biol. Appl.* **2013**, *33*, 3576–3582.

Submitted: March 31, 2019
Accepted: May 20, 2019